Characterization of Carbon Nanofiber Electrode Arrays Using Electrochemical Impedance Spectroscopy: Effect of Scaling Down Electrode Size

Shabnam Siddiqui, Prabhu U. Arumugam,* Hua Chen, Jun Li,† and M. Meyyappan

NASA Ames Research Center, Moffett Field, California 94035. †Current address: Department of Chemistry, Kansas State University, Manhattan, Kansas 66506

ABSTRACT We report here how the electrochemical impedance spectra change as (i) electrode size is reduced to nanometer scale and (ii) spacing between vertically aligned carbon nanofiber (VACNF) electrodes is varied. To study this, we used three types of electrodes: standard microdisks (100 μm Pt, 10 μm Au, and 7 μm glassy carbon), randomly grown (RG) VACNFs where spacing between electrodes is not fixed, and electron beam patterned VACNF nanoelectrode arrays (pNEAs) where electrode spacing is fixed at 1 μm. As the size of the microdisk electrode is reduced, the spectrum changed from a straight line to a semicircle accompanied by huge noise. Although a semicircle spectrum can directly indicate the electron transfer resistance (R_{ct}) and thus is useful for biosensing applications, the noise from electrodes, particularly from those with diameters ≤10 μm, limits sensitivity. In the case of VACNFs, the electrode spacing controls the type of spectrum, that is, a straight line for RG VACNFs and a semicircle for pNEAs. In contrast to microdisks, pNEAs showed almost insignificant noise even at small perturbations (10 mV). Second, only pNEAs showed linearity as the amplitude of the sinusoidal signal was increased from 10 to 100 mV. The ability to apply large amplitudes reduces the stochastic errors, provides high stability, and improves signal-to-noise (S/N) ratio. This new class of nanoelectrochemical system using carbon pNEAs offers unique properties such as semicircle spectra that fit into simple circuits, high S/N ratio, linearity, and tailor-made spectra for specific applications by controlling electrode size, spacing, and array size.

KEYWORDS: carbon nanofibers · electrochemical impedance spectroscopy · nanoelectrode array · ultrasensitive nucleic acid detection · biosensor · linearity

Electrochemical impedance spectroscopy (EIS) is one of the most effective techniques for studying the properties at the electrode−electrolyte interface. It is used in a wide range of applications like label-free biosensors,[1,2] corrosion, coatings, cell culture monitoring and screening,[3] and electrode performance studies in fuel and solar cells. In EIS, the system under study is subjected to perturbations by applying a sinusoidal voltage of small amplitudes (5−10 mV) with variable frequency (0.1 Hz to 100 kHz), and the resulting change in impedance (Z) is measured. The imaginary impedance (Z_{Im}) and the real impedance (Z_{Re}) are recorded as a function of the applied frequency. By fitting the resulting Nyquist plot (Z_{Im} *vs* Z_{Re}) to simple circuits, important information of the interface such as electron transfer resistance (R_{ct}), solution resistance (R_s), double layer capacitance (C_{dl}), and Warburg element (R_w) is measured. Typically, three types of Nyquist plots are observed in electrochemical systems: (1) a straight line, which represents a diffusion-limited process with facile electron transfer; (2) a semicircle accompanied by a straight line at the low-frequency region of the spectrum; and (3) a semicircle, which represents electron transfer-limited process. The diameter of the semicircle (*x*-axis) corresponds to the R_{ct} at the electrode. For biosensor applications, a semicircle spectrum with negligible noise from a bare, unmodified electrode is preferable as it provides higher sensitivity.

Various groups have employed EIS for DNA and enzyme-based[4,5] sensors, where a modification of the electrode by immobilization of probes and target biomolecules changes the R_{ct} and C_{dl} of the electrode interface. This change in response is measured and rendered as detection. Unlike other electrochemical techniques, EIS has several advantages such as specificity, sensitivity, rapidity, and low cost, all of which are important for successful field implementation. The most commonly used electrodes for biosensing are bare and modified macro- and microdisk electrodes made from noble metals. The electrodes are modified (for example, with nanoparticles[6,7]) to enhance the sensitivity, which requires additional steps and adds to cost and time. Recently, one-dimensional (1D) electrode materials such as carbon nanotubes (CNTs),[8] carbon nanofibers (CNFs),[9,10] silicon nanowires,[11] and diamond nanowires[12] were explored as alternatives to build better

*Address correspondence to prabhu.u.arumugam@nasa.gov

Received for review June 25, 2009 and accepted January 12, 2010.

Published online January 25, 2010. 10.1021/nn901583u

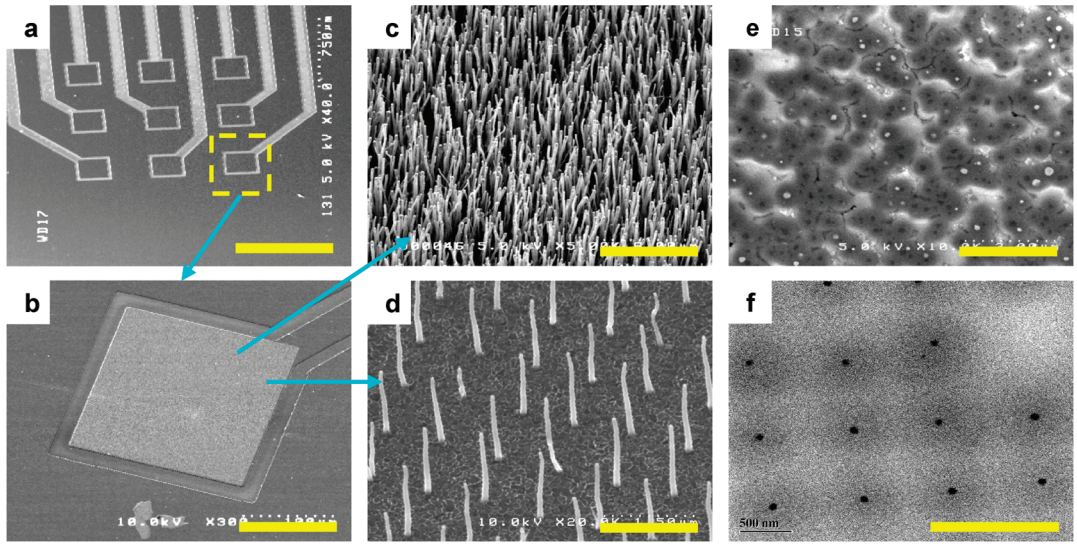

Figure 1. Fabrication of VACNF chips. SEM images of (a) 3 × 3 array chip, (b) one individual array with VACNF growth, (c) as-grown randomly grown (RG) VACNFs, (d) as-grown nanopatterned VACNF on 100 nm diameter Ni catalyst spots, (e,f) surface of a polished RG and nanopatterned VACNFs embedded in SiO_2 matrix; (c,d) 30° perspective views, (a,b,e,f) top views. The scale bars are (a) 750, (b) 100, (c) 6, (d) 1.5, (e) 3, and (f) 1 μm.

electrochemical sensors. Such nanoscale electrodes exhibit radial diffusion dominant behavior providing higher sensitivity and low limits of detection using ultrasmall volumes, but not many studies have been conducted that provide similar understanding for EIS techniques. A recent review[13] underlined the importance of understanding the effect of scaling down electrode size for impedance-based biosensing. Here we studied how the impedance spectra (Nyquist plot) change as (i) electrode size is reduced to nanometer scale and (ii) spacing between vertically aligned carbon nanofiber (VACNF) electrodes is varied. We used three types of electrodes: standard microdisks (100 μm Pt, 10 μm Au, and 7 μm glassy carbon electrode, GCE), randomly grown (RG) VACNFs where spacing between electrodes is not fixed (Figure 1c,e), and e-beam patterned VACNF nanoelectrode arrays (pNEAs) where spacing is fixed at 1 μm (Figure 1d,f). VACNFs were grown on a 3 × 3 array chips (Figure 1a) using plasma-enhanced chemical vapor deposition (Figure 1b). In this work, we present the characteristics of impedance spectra of RG and pNEA chips that were systematically compared with microdisk electrodes in terms of spectra shape, linearity, electrode size, potential, electrode kinetics, and signal/noise (S/N) ratio.

RESULTS AND DISCUSSION

Electrochemical properties of bare, unmodified VACNF chips were evaluated through cyclic voltammetry (CV) and impedance spectroscopy (EIS). The electrochemically etched VACNFs (for more details, refer to the Methods section) can be approximately treated as inlaid nanodisk electrodes. From SEM images, the density of exposed CNFs and the average nearest-neighbor distance for high-density RG chips is ~2×10^9 electrodes cm^{-2} and ~125 nm. For low-density and ultra-low-density chips, it is ~6.5×10^7 and ~9×10^6 electrodes cm^{-2}, and the nearest-neighbor distance is fixed at 1 μm by e-beam patterning. The low- and ultra-low-density pNEAs are etched for 15 and 30 s, respectively. We observed that, with longer etch time, more carbon atoms were removed from the fiber tip, resulting in lower currents and shallower fibers, that is, recessed from the SiO_2 surface. The CV from high-density RG chips (Figure 2a) shows a macroelectrode behavior with anodic and cathodic peak currents and high charging/discharging (background) currents. This is expected because they were grown from a continuous Ni catalyst film where spacing between exposed VACNFs was not fixed; consequently, the average interspacing between them is lower than twice that of the steady-state diffusion layer of an individual nanoelectrode by empirical estimation (*i.e.*, ~$6R_{ave} \approx 300$ nm, where $R_{ave} = \sim 50$ nm is the average electrode radius). In contrast, pNEAs prepared from e-beam patterned 100 nm diameter Ni catalyst dots provide a well-controlled spacing of 1 μm, which is much larger than $6R_{ave}$. This ensures that there is no overlap of the radial diffusion layers from neighboring electrodes and each CNF truly behaves as a single nanoelectrode showing a sigmoidal CV curve with the steady-state current dominated by radial diffusion (Figure 2c,e). Such arrays are preferred for ultrasensitive biomolecule detection because of their high S/N ratio.[14] The question we need to ask is whether pNEAs can offer similar sensitivity using EIS technique. In this work, we explored the electrochemical properties of pNEAs as a first step toward answering this question.

Effect of Electrode Spacing of VACNFs on Impedance Spectra. Figure 2b,d,f shows the impedance spectra of high-density RG, low-density pNEAs, and ultra-low-density pNEAs at 0 V dc potential *vs* saturated calomel electrode (SCE), respectively. The spectrum of high-density

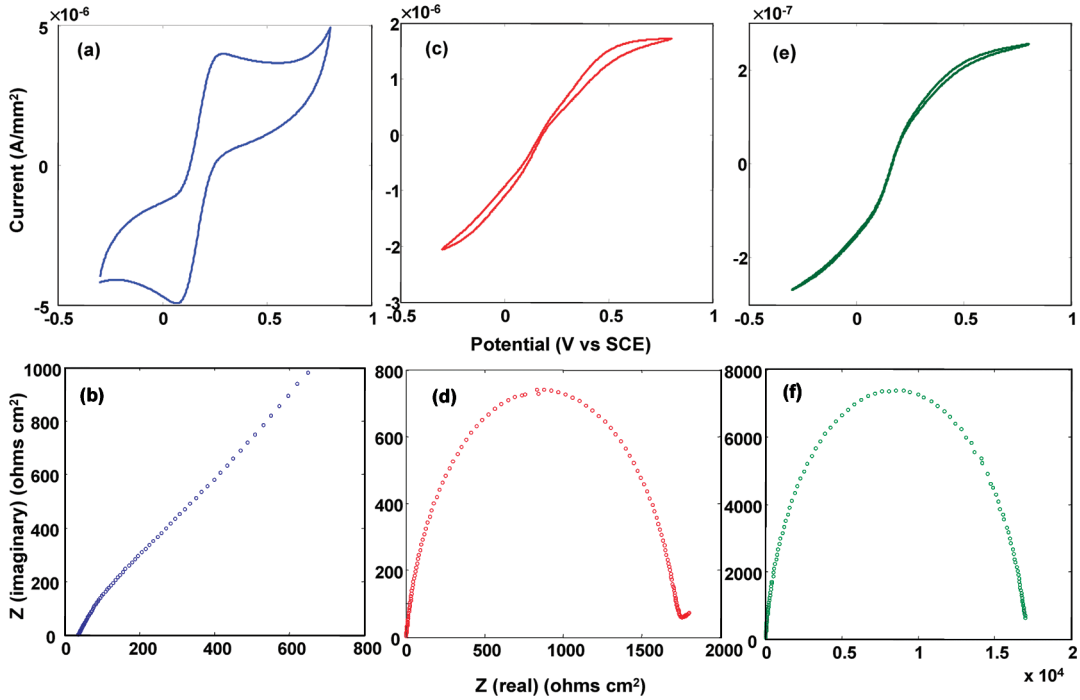

Figure 2. CV and EIS spectra of different types of carbon nanofiber (CNF) chips. (a,c,e) CV and (b,d,f) impedance curves of high, low, and ultralow density VACNF chips, respectively. A solution of 5 mM $K_4Fe(CN)_6$/5 mM $K_3Fe(CN)_6$ in 0.1 M phosphate buffer (pH 7.4) (1:1 mixture) was used. CVs were taken at 20 mV/s scan rate. Impedance spectra were taken at 10 mV, 0.1 Hz to 100 kHz, and 0 V dc potential *vs* SCE.

RG is a monotonically increasing straight line, and this linear correlation between Z_{Im} and Z_{Re} corresponds to diffusion-limited process. The spectra of low-density pNEAs consist of a large semicircle (charge transfer-limited) with a very small straight line (diffusion-limited) in very low frequency range known as Warburg element. By reducing the density of CNF electrodes in an array further (*i.e.*, ultra-low-density pNEAs), the spectrum changes to just a semicircle and no Warburg element is observed (Figure 2f). This demonstrates that by choosing the right electrode size, electrode spacing, and array size, the impedance spectra can be changed from "straight line" to "semicircle" feature. The main advantage of semicircle behavior is that it can be described through a simple Randles circuit (Figure 3, inset). The semicircle obtained through experimental data perfectly fits the circuit model (Figure 3). Hence the value of each component of the system (R_s, C_{dl}, and R_{ct}) can be readily obtained using the model. The semicircle spectrum from bare pNEAs is very useful for biosensing applications because one can observe a direct change in the value of R_{ct} upon binding of probes. This allows one to perform quantitative studies of probe lengths and probe concentrations for sensor development.

We observed that, by applying a more positive dc potential (+0.3 V), R_{ct} decreases and a more negative dc potential (−0.3 V) causes an increase in R_{ct} when compared with 0 V dc potential (data not shown). Table 1 lists the fitting parameters for the EIS data of the three types of VACNF chips. The constant phase element (CPE) decreases due to reduction in active electrode area, and its behavior is close to an ideal capaci-

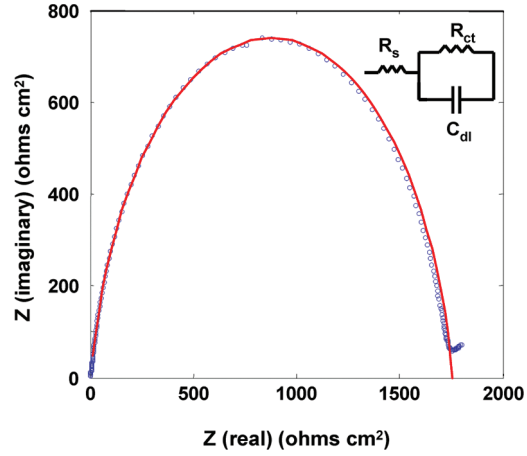

Figure 3. Comparison of actual and fitted impedance spectrum of a low-density VACNF chip. The experimental data (open circles) fit perfectly to the fitted curve (solid curve) based on Randles circuit (inset). A solution of 5 mM $K_4Fe(CN)_6$/5 mM $K_3Fe(CN)_6$ in 0.1 M phosphate buffer (pH 7.4) (1:1 mixture) was used. The spectra were taken at 10 mV, 0.1 Hz to 100 kHz, and 0 V dc potential *vs* SCE.

TABLE 1. Fitting Parameters for the EIS Data of Three Types of VACNF Chips

	RG CNF	NEA (low density)	NEA (ultralow density)
I (A/mm²)	7.1×10^{-6}	1.8×10^{-6}	2.5×10^{-7}
R_{ct} (KΩ)	N/A	1.8	17.3
CPE (μF)	906	3.3	2.5
n	0.79	0.89	0.91

TABLE 2. Effect of Scaling Down Electrode Dimensions on the Characteristic of Impedance Spectra

electrode type and dimension	I (A)	I (A/mm^2)	characteristic of Impedance Spectra
RG CNF (*high density*)	28×10^{-6}	4.0×10^{-6}	straight line (Figure 2b)
100 μm Pt	200×10^{-9}	25×10^{-6}	partial semicircle with Warburg element (Figure 5b)
NEA CNF (low density)	75×10^{-9}	1.8×10^{-6}	semicircle with a small Warburg element (Figure 2d)
7 μm GCE	7.7×10^{-9}	193×10^{-6}	semicircle (Figure 5c)
NEA CNF (ultralow density)	10×10^{-9}	0.25×10^{-6}	semicircle (Figure 2f)

tor as shown by the value of n, where n is the number of electrons transferred per molecule of the redox probe. CPE reflects nonhomogeneity of the electrode surface and is given by $A^{-1}\ (j\omega)^{-n}$, where A is capacitance. When $n = 1$, A becomes equal to C_{dl} (ideal capacitor).

We observed an increase in R_{ct} as the number of CNFs (electrode area) is reduced. From Figure 2d,f, the R_{ct} of low and ultralow density is 4.4 and 42 MΩ, respectively. This increase in the value of R_{ct} is due to reduction in exchange current under equilibrium I_0, as shown in eqs 1 and 2.[16] Now, from eq 2, I_0 decreases due to reduction in effective electrode area (A), assuming k is constant. The effective area is defined as the number of fibers times the area of an individual fiber, assuming the diameter of all the fibers are the same.

$$R_{ct} = \frac{RT}{nFI_0} \quad (1)$$

$$I_0 = nFAkC \quad (2)$$

where R is molar gas constant (8.31447 J mol^{-1} K^{-1}), T is temperature (K), n is stoichiometric number of electrons involved in an electrode reaction, F is the Faraday constant, A is area of electrode, k is electron transfer rate constant, and C is concentration of the redox probes. Thus by controlling the electrode area and k through careful electrode fabrication, one can obtain desirable values of R_{ct} as required for biosensing applications.

Effect of Electrode Size on the Impedance Spectra of Microdisks Electrodes. We performed similar studies using microdisk electrodes. Table 2 summarizes the overall effect of electrode size on impedance spectra. We observed that the spectra change from a Warburg-type spectrum to that of a semicircle as one reduces the size of microdisks. Though the electrode materials used are different, our study shows that, for 10 μm Au and 7 μm GCE, the impedance spectra are similar with a semicircle behavior (data not shown). Hence, electrodes made of Pt, Au, and GCE with similar dimensions exhibit similar impedance spectra. Here, the focus is to observe change in impedance spectra as one reduces the electrode size irrespective of the material used. In addition, we observed huge noise (scattered data points) at low frequencies from electrodes (≤10 μm diameters) in spite of careful electrode preparation and well-defined CV signals. Similar observations have been reported previously.[16] In contrast, pNEAs show almost insignificant noise at low frequencies even at small perturbations (10 mV) and are well-suited for sensitive impedance measurements.

Effect of Electrode Size and Spacing of pNEAs on Linearity. Electrochemical impedance spectra have a meaningful interpretation only if the electrochemical cell behaves linearly; that is, impedance is independent of amplitude of the applied voltage (also called linearity). Typically, an electrochemical cell can be represented by a circuit model of a resistance in series with a capacitor. When a voltage (V) is applied across this circuit, the total voltage drop is equal to the sum of the individual voltage drops across the resistor and the capacitor, thus

$$\dot{V} = \dot{V}_R + \dot{V}_C \rightarrow \dot{V} = \dot{I}(R - jX_c) \rightarrow \dot{V} = \dot{I}Z \quad (3)$$

where $\dot{V}$ is rate of change of voltage, $\dot{I}$ is rate of change of current, $Z = R - jX_c$, and $X_c = 1/\omega C$ is capacitive reactance.[15] It can be seen from this expression that the only variable impedance depends on the frequency of the applied voltage. In the impedance spectra (Nyquist plot), ideally one should not observe any change as the amplitude of the applied voltage is varied. However, electrochemical cells are nonlinear, and therefore, such an ideal behavior is not observed. In order to maintain linearity of the cell during the measurement process, an ac signal of very small amplitude is generally applied, but such small amplitudes give rise to poor S/N ratio and is not suitable for sensitive measurements. One way to reduce the noise is to increase the amplitude of the applied voltage, but this introduces nonlinearity into the system, which makes it difficult to interpret the spectrum using simple circuit models. In most studies, it was shown that impedance data are meaningful only when ac signal of amplitude ≤25 mV is applied.[17,18] Large amplitudes give rise to higher harmonics[15,19] and thus cause nonlinearity. For biosensor applications, a larger microelectrode with very low amplitudes (~10 mV) is typically used.

Previously, we observed high S/N ratio from pNEAs using voltammetry techniques.[14] This motivated us to investigate pNEAs for linearity at large amplitudes. In this work, we systematically studied the linearity by increasing the amplitude from 10 to 200 mV but with fixed frequency range (0.1 Hz to 100 kHz). Figure 4a, curve I, shows the CV, and Figure 4b shows the EIS spectra from one of the arrays at different amplitudes with 0 V dc signal *vs* SCE. The spectrum, in general, is a semi-

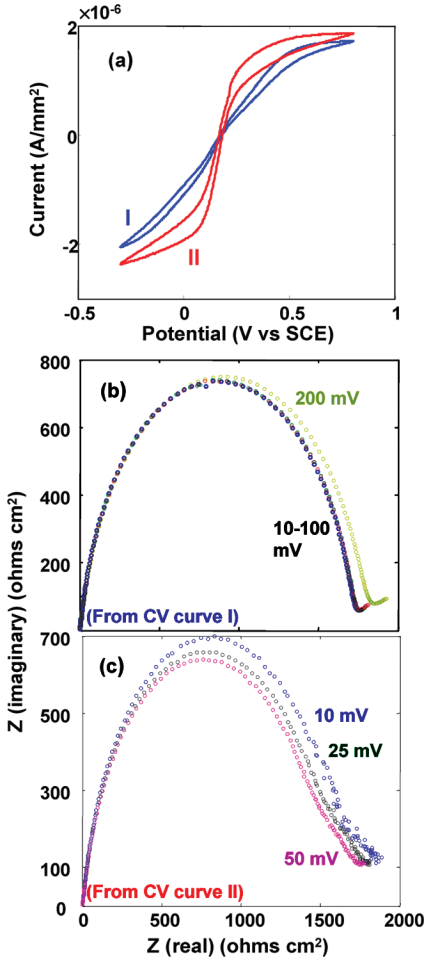

Figure 4. Effect of electrode kinetics of pNEAs on linearity. (a) CV curves of *sss*- (blue curve) and *fss*-pNEAs (red curve). (b) Impedance curves of *sss*-pNEAs at different amplitudes (10, 25, 50, 75, 100, and 200 mV). (c) Impedance curves of *fss*-pNEAs at different amplitudes (10, 25, and 50 mV). A solution of 5 mM $K_4Fe(CN)_6$/5 mM $K_3Fe(CN)_6$ in 0.1 M phosphate buffer (pH 7.4) (1:1 mixture) was used. The spectra were taken at 0.1 Hz to 100 kHz and 0 V dc potential *vs* SCE.

circle with a very small (almost negligible) Warburg element. All of the spectra for amplitudes 10−100 mV are perfectly the same, and each of them completely overlays. This implies that there is no change in the value of impedance as the amplitude of the applied signal is increased to 100 mV, thus pNEAs show linearity. We have repeated the experiments several times under the same conditions using different arrays on different days and found the results to be reproducible. We always observed a semicircle spectrum and linearity except for the variations in the values of the interfacial properties, which is due to the difference in the density of fibers from the arrays and fabrication inconsistencies. By increasing the amplitude further to 200 mV, a shift is observed at lower frequencies; hence the system starts to behave nonlinearly. This makes NEAs a unique system where, due to the array pattern and nanosize of the electrodes, a new electrochemical property like linearity was observed even at large amplitudes.

Some of the other interesting observations that are characteristic of pNEAs include the following: (i) Linearity of the cell is a potential dependent phenomenon as expected.[20] By making dc potential more positive or negative, linearity is not observed (data not shown). The system is linear only when 0 V dc potential *vs* SCE is applied. (ii) Linearity of the cell is an electrode kinetics dependent phenomenon. Even though all nine arrays in an NEA chip are identically prepared, we observed two types of CV curves with same amplitudes of the limiting current from these arrays (*i.e.*, the number of VACNFs exposed or the total surface area of the VACNFs are about the same between the arrays), one where the steady-state currents are reached slowly, henceforth called slow steady state pNEAs (*sss*-pNEAs) (Figure 4a, curve I), and others where it reached faster, henceforth called fast steady state pNEAs (*fss*-pNEAs) (Figure 4a, curve II). The origin of this variation in electrode kinetics may be likely due to the difference in resistance between the arrays in the same chip, arising from the inhomogeneity in CNF height and array density and electrode surface preparation. These are issues critical to large wafer manufacturing to be addressed later. Interestingly, by using $Fe(CN)_6^{3-/4-}$, which is sensitive to surface defects or impurities,[21] we were able to understand the importance of electrode surface conditions necessary to achieve linearity. We found that linearity is observed only in those arrays where the steady-state currents are reached slowly (Figure 4b) and not with the ones where it is reached faster (Figure 4c). Thus, the electrode history (*i.e.*, fabrication and activation steps) plays an important role in observing linearity in carbon-based nanoelectrode arrays. This prompts us to ask whether linearity can be observed from similar NEAs made from noble metal electrodes, which exhibits facile kinetics. In addition, we also observed that the spectrum of *fss*-pNEAs is accompanied by noise at low frequencies for small amplitudes, ≤25 mV (Figure 4c). This noise might have been the cause for nonlinearity, which is currently under investigation. We conclude that *sss*-pNEAs with no noise are the most suitable electrode platform for biosensing applications. (iii) Linearity is not observed for RG CNFs and microdisk electrodes (Figure 5a−c). Also, Figure 5c shows the huge noise from GCE as discussed before. We suggest that *sss*-pNEAs can be a potential candidate for high amplitude EIS studies like DNA switching.[22] Our lab is currently working on understanding how electrode dimensions and kinetics play an important role in observing linear systems. We believe there is a tremendous need to study such nanoelectrode systems within theoretical and experimental framework to facilitate the use of nanomaterials for new applications.

CONCLUSIONS

As one scales down the electrode dimensions from micrometers to nanometers, impedance spectra change

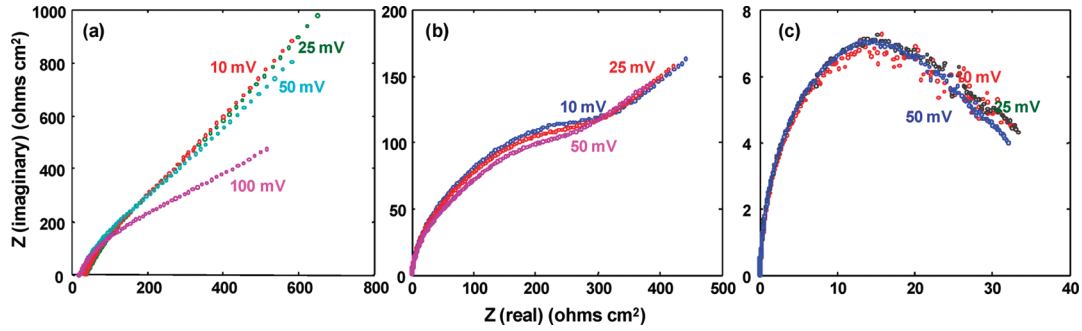

Figure 5. Linearity at different types of electrodes. (a) Randomly grown VACNFs, (b) 100 μm Pt, and (c) 7 μm GCE. Impedance curves were taken at different amplitudes (10, 25, 50, and 100 mV). A solution of 5 mM $K_4Fe(CN)_6$/5 mM $K_3Fe(CN)_6$ in 0.1 M phosphate buffer (pH 7.4) (1:1 mixture) was used. The spectra were taken at 0.1 Hz to 100 kHz and 0 V dc potential *vs* SCE.

from a straight line to a semicircle. Hence, by controlling electrode size, electrode spacing, and array size, impedance spectra can be tailored for specific applications. VACNF pNEAs offer unique advantages such as perfect semicircle behavior that fits Randles circuit, low noise, and linearity at larger amplitudes (>25 mV), which has not been demonstrated before. The pNEA-based EIS is a better and well-suited technique for biosensing applications and kinetic studies because it offers higher sensitivity and stability. The ability to use large amplitudes using pNEAs will open up new applications for this emerging class of 1D carbon nanostructures.

METHODS

Fabrication of VACNF Nanoelectrode Arrays. The details of the fabrication of VACNF arrays are discussed in ref 14. Briefly, a 4 in. wafer with 30 sensor chips is fabricated. Each chip contains nine individually addressable micropad arrays (3 × 3 format, 200 μm squares) that use electron beam patterned vertically aligned carbon nanofibers (VACNFs) as the sensing element. The underlying oxide electrically isolates all nine micropads. All processes are done on a 4 in. silicon (100) wafer coated with 500 nm thick thermal oxide (Silicon Quest International, Inc., Santa Clara, CA). The six major steps for the wafer-scale fabrication of e-beam patterned VACNF NEAs are (1) optical lithography patterning and electron beam metal deposition (200 nm Cr film) of micropads, contact pads, and electrical interconnects (Figure 1a); (2) nanopatterning of Ni catalyst dots where a single micropad consists of ~39 000 catalyst dots with 100 ± 30 nm diameters; (3) dc-biased PECVD growth of VACNFs with C_2H_2 feedstock (125 sccm) and NH_3 diluent (444 sccm) at 6.3 mbar, 700 °C and 180 W (Figure 1d); a 5 min thermal annealing at 600 °C was performed before initiating the plasma with 250 sccm NH_3; each CNF was vertically aligned and free-standing on the surface with Ni catalyst at the tip, and a 15 min deposition yielded, on average, a height of ~1.5 μm, a base diameter of ~100 nm, and a tip diameter of ~80 nm; (4) silicon dioxide deposition for electrical isolation and mechanical support; (5) chemical mechanical polishing (CMP) to expose CNF tips (Figure 1f); and (6) a wet etch with 7:1 HF to expose contact pads. The wafers were diced into individual chips of ~14 mm squares in size. The details of the different process steps are discussed elsewhere.[14] The scanning electron microscope images were taken using S4160 field emission SEM (Hitachi, Japan) operated at an acceleration voltage in the range of 7−10 kV. For RG high-density chips, all of the above steps were followed except that a 30 nm thick Ni continuous film was used as a catalyst instead of nanodots on the 200 nm Cr squares.

Electrochemical Characterization Measurements. All EC experiments were carried out with an Autolab potentiostat (GPSTAT12, Ecochemie, Netherlands) in a three-electrode setup using a Pt coil counter electrode and a saturated calomel electrode (SCE, Accumet, New Hampshire, USA) as the reference electrode. The embedded NEAs on individual micropads (Figure 1b) were used as the working electrode. Only the micropad arrays were exposed to the solution sealed with a 3 mm i.d. O-ring in a Teflon cell. For each sensor array chip, the electrical isolation of the pads was checked using a multimeter. This ensures the integrity of the SiO_2 passivation, which is essential for stable sensors. The cyclic voltammograms (CV) were recorded between −0.3 and + 0.8 V *vs* SCE with a scan rate of 20 mV/s in a solution of 5 mM $K_4Fe(CN)_6$/5 mM $K_3Fe(CN)_6$ in 0.1 M phosphate buffer (pH 7.4) (1:1 mixture). Prior to electrochemical characterization, VACNFs were pretreated by the combination of soaking in 1.0 M HNO_3 and etching in 1.0 M NaOH for several reasons including removal of damages, if any, to the VACNF tips during various microfabrication processes, improving electrode kinetics, preserving the nanoelectrode behavior, and introducing −COOH groups for subsequent covalent binding of the oligonucleotide probes for biosensor development.[14] After pretreatment, the electrode performance dramatically improved as indicated by the decrease of redox peak separation (ΔE_p) to ~100 mV and an approximately 200% increase in steady-state currents. All commercial electrodes were manually polished using 0.3 and 0.05 μm Alpha micropolish alumina, respectively (Buehler, Lake Bluff, IL), and sonicated in distilled water for 2 min before the experiments. All data were normalized to the geometric area, which is 7.065 mm^2 for high-density chips based on the 3 mm opening of the electrochemical cell and 0.04 mm^2 for low and ultralow density based on 200 μm square pads. Note: In Figure 2a, the normalized current for RG chips is only ~2× that of low-density pNEAs, but the actual current values varied by ~1000×. This discrepancy is due to a huge difference between the geometric and effective area of RG and pNEA chips. Therefore, a meaningful comparison of current densities can be made only between low and ultralow density pNEAs.

Electrochemical Impedance Spectroscopy (EIS) Measurements. EIS measurements were carried out in a mixture of 5 mM $K_4Fe(CN)_6$ and 5 mM $K_3Fe(CN)_6$ in 0.1 M phosphate buffer (pH 7.4) using a GPSTAT12 potentiostat/galvanostat equipped with a frequency response analyzer module (FRA 4.9.007 version). The impedance spectra were recorded between 100 kHz and 0.1 Hz at different ac signal amplitudes (rms value) (10, 25, 50, 70, 100, and 200 mV).

Acknowledgment. This work was funded by EarlyWarning Inc., Troy, NY, *via* contract number NAS2-03144 (Task TO.066.0.HP.TSN) to NASA Ames Research Center, University Affiliated Research Center (UARC), University of California, Santa Cruz and Eloret Corporation. P.U.A. and H.C. are employed by ELORET Corporation; S.S. is employed by Education Associates, onsite contractors at NASA Ames. We thank M. Pujado, J.A.P. Weinrich, and A. Jejelowo for their help with the experiments.

REFERENCES AND NOTES

1. Yun, Y. H.; Shanov, V.; Schulz, M. J.; Dong, Z.; Jazieh, A.; Heineman, W. R.; Halsall, H. B.; Wong, D. K. Y.; Bange, A.; Tu, Y.; Subramaniam, S. High Sensitivity Carbon Nanotube Tower Electrodes. *Sens. Actuators, B* **2006**, *120*, 298–304.
2. Yun, Y. H.; Bange, A; Heineman, W. R.; Halsall, H. B.; Shanov, V.; Dong, Z.; Pixley, S.; Behbehani, Jazieh, A.; Tu, Y.; Wong, D. K. Y.; Bhattacharya, A.; M.; Schulz, A. Nanotube Array Immunosensor for Direct Electrochemical Detection of Antigen−Antibody Binding. *Sens. Actuators, B* **2007**, *123*, 177–182.
3. K'Owino, I. O.; Sadik, O. A. Impedance Spectroscopy: A Powerful Tool for Rapid Biomolecular Screening and Cell Culture Monitoring. *Electroanalysis* **2005**, *17*, 2101–2113.
4. Long, Y. T.; Li, Z.-C.; Kraatz, H.-B.; Lee, J. S. AC Impedance Spectroscopy of Native DNA and M-DNA. *Biophys. J.* **2003**, 3218–3225.
5. Guan, J. G.; Miao, Y. Q.; Zhang, Q. J. Impedimetric Biosensors. *J. Biosci. Bioeng.* **2004**, *97*, 219–226.
6. Wang, M.; Wang, L.; Wang, G.; Ji, X.; Bai, Y.; Li, T.; Gong, S.; Li, L. Application of Impedance Spectroscopy for Monitoring Colloid Au-Enhanced Antibody Immobilization and Antibody−Antigen Reactions. *Biosens. Bioelectron.* **2004**, *19*, 575.
7. Fu, Y.; Yuan, R.; Xu, L.; Chai, Y.; Liu, Y.; Tang, D.; Zhang, Y. Electrochemcial Impedance Behavior of DNA Biosensor Based on Colloidal Ag and Bilayer Two-Dimensional Sol−Gel as Matrices. *J. Biochem. Biophys. Methods* **2005**, *62*, 163–174.
8. Yun, Y. H.; Dong, Z.; Shanov, V. N.; Schulz, M. J. Electrochemical Impedance Measurement of Prostate Cancer Cells Using Carbon Nanotube Array Electrodes in a Microfluidic Channel. *Nanotechnology* **2007**, *18*, 465505.
9. Li, J.; Koehne, J.; Cassell, A. M.; Chen, H.; Ye, Q.; Ng, H. T.; Han, J.; Fan, W.; Meyyappan, M. Inlaid Multi-Walled Carbon Nanotube Nanoelectrode Arrays for Electroanalysis. *Electroanalysis* **2005**, *17*, 15–27.
10. Li, J.; Ng, H. T.; Cassell, A. M.; Fan, W.; Chen, H.; Koehne, J.; Han, J.; Meyyappan, M. Carbon Nanotube Nanoelectrode Array for Ultrasensitive DNA Detection. *Nano Lett.* **2003**, *3*, 597–602.
11. Patolsky, F.; Zheng, G.; Lieber, C. M. Fabrication of Silicon Nanowire Devices for Ultrasensitive, Label-Free, Real-Time Detection of Biological and Chemical Species. *Nat. Protoc.* **2006**, *1*, 1711–1724.
12. Yang, N.; Uetsuka, H.; Osawa, E.; Nebel, C. E. Vertically Aligned Diamond Nanowires for DNA Sensing. *Angew. Chem., Int. Ed.* **2008**, *47*, 5183–5185.
13. Daniels, J. S.; Pourmand, N. Label-Free Impedance Biosensors: Opportunities and Challenges. *Electroanalysis* **2007**, *19*, 1239–1257.
14. Arumugam, P. U.; Chen, H.; Siddiqui, S.; Weinrich, J. A. P.; Jejelowo, A.; Li, J.; Meyyappan, M. Wafer-Scale Fabrication of Patterned Carbon Nanofiber Nanoelectrode Arrays: A Route for Development of Multiplexed, Ultrasensitive Disposable Biosensors. *Biosens. Bioelectron.* **2009**, *24*, 2818–2824.
15. Bard, A. J.; Faulkner, L. R. *Electrochemical Methods: Fundamentals and Applications*; John Wiley & Sons, Inc: New York, 2001; pp 368−388.
16. Bruce, P. G.; Oleksiak, A. L.; Los, P.; Vincent, C. A. Electrochemcial Impedance Spectroscopy at an Ultramicroelectrode. *J. Electroanal. Chem.* **1994**, *367*, 279–283.
17. Barbero, G.; Alexe-Ionescu, A. L.; Lelidis, I. Significance of Small Voltage in Impedance Spectroscopy Measurements on Electrolytic Cells. *J. Appl. Phys.* **2005**, *98*, 1137031–1137035.
18. Freire, F. M.; Barbero, G.; Scalerandi, M. Electrical Impedance for an Electrolytic Cell. *Phys. Rev. E.* **2006**, *73*, 051202–051211.
19. Darowicki, K. The Amplitude Analysis of Impedance Spectra. *Electrochim. Acta* **1995**, *40*, 439–445.
20. Mark E. Orazen and Bernard Tribollet. *Electrochemical Impedance Spectroscopy*; John Wiley & Sons: New York, 2008; p 134.
21. Huang, W; McCreery, R. L. Electron Transfer Kinetics of $Fe(CN)^{z-/4-}$ on Laser-Activated and CN-Modified Pt Electrodes. *J. Electroanal. Chem.* **1992**, *326*, 1–12.
22. Rant, U.; Pringsheim, E.; Kaiser, W.; Arinaga, K.; Knezevic, J.; Tornow, M.; Fujita, S.; Yokoyama, N.; Abstreiter, G. Detection and Size Analysis of Proteins with Switchable DNA Layers. *Nano Lett.* **2009**, *9*, 1290–1295.